CANADIAN JOURNAL OF EXPLORATION GEOPHYSICS
VOL. 24, NO. 1 (JUNE 1988), P. 16-31

PRACTICAL AND EFFICIENT RAY TRACING IN TWO-DIMENSIONAL MEDIA FOR RAPID TRAVELTIME AND AMPLITUDE FORWARD MODELLING

C.A. ZELT[1] AND R.M. ELLIS[1]

ABSTRACT

An algorithm for tracing rays and calculating amplitudes in two-dimensional media based on a new velocity-model parameterization has been developed. The simple, layered, large-block parameterization in which velocity is an analytic function of position allows for computationally efficient ray tracing. The user's ability to specify simple kinematically similar ray families permits practical and rapid forward modelling of refraction data. In addition, the routine allows for *S*-wave propagation including converted phases, multiple and surface reflections, approximate attenuation, head waves, and a reverse ray-direction amplitude calculation important for the interpretation of common-receiver profiles. The source may emit both *P*- and *S*-type rays and the ratio of *P*-wave to *S*-wave amplitude at the source may be specified. Amplitude calculations are based on zero- and first-order asymptotic ray theory.

The velocity model is parameterized in terms of a sequence of quasi-horizontal layers, each layer separated by a boundary consisting of straight-line segments. Layer thicknesses may be reduced to zero to model pinch-outs or isolated bodies. Each layer is broken up laterally into a series of large trapezoidal blocks with vertical left and right sides and upper and lower boundaries of arbitrary dip. The velocity structure within each trapezoid is defined by a single upper and lower velocity such that the velocity varies linearly from the upper to lower boundary along a vertical path.

The major attributes of the routine are illustrated with four examples: a comparison of efficiency and accuracy with the Spence et al. algorithm, a practical application to the interpretation of observed crustal refraction profiles from the Peace River Arch region, a complex subduction zone model to illustrate the degree of lateral inhomogeneity possible with the routine's model parameterization, and a demonstration of how the routine may be used to study the effects of near-surface velocity anomalies on CMP data.

INTRODUCTION

The interpretation of crustal seismic refraction data is generally carried out using a trial-and-error forward-modelling approach based on two-dimensional ray tracing (e.g., Spence et al., 1985; Mereu et al., 1986; Meltzer et al., 1987). The theoretical traveltime and amplitude response of a laterally inhomogeneous medium are repeatedly compared with observed record sections until a model is constructed which provides a satisfactory match between calculation and observation. This iterative, forward-modelling approach is necessary because no inversion scheme exists which is capable of providing geologically reasonable models in laterally varying media for a typical crustal refraction data set. Thus, an appropriate algorithm for forward modelling must be capable of accurately calculating the traveltimes and amplitudes associated with a general two-dimensional model in an efficient and practical manner to allow for many trials.

A number of algorithms based on asymptotic ray theory (Červený et al., 1977) have been developed and widely used, each satisfying the above-mentioned requirements to varying degrees. These algorithms include those of McMechan and Mooney (1980), Červený and Pšenčík (1981), Cassell (1982) and Spence et al. (1984). Numerous more accurate but less efficient techniques for forward modelling in one-, two- and three-dimensional media exist and are necessary for detailed studies of particular wave-propagation problems and as a final check on models obtained using the ray method; however, routines based on the ray method are at present the only economical and practical choice for the interpreting seismologist. This paper presents a routine based on the ray method which possesses similar advantages and limitations of other algorithms but offers greater practicality.

The fundamental feature of the new routine is its simple, layered, large-block velocity model parameterization. This allows for efficient ray tracing. And since one requires a minimum number of parameters to define the model completely, changes to it can be made quickly by the user. Rapid forward modelling is achieved by allowing the user to select simple kinematic ray families for exploring a part of the model of interest. In addition, a

Manuscript received by the Editor November 30, 1987; revised manuscript received March 17, 1988.

[1]Department of Geophysics and Astronomy, University of British Columbia, Vancouver, B.C. V6T 1W5

The authors would like to thank A.V. Boland, C.F. Cudrak and D.E. Lumley for suggesting improvements to the computer programs and D.J. White for useful discussions on ray theory and ray tracing. Additional thanks to D.E. Lumley for help with the CMP example. A critical review by R.M. Clowes is gratefully acknowledged. This research has been funded by the Institute of Sedimentary and Petroleum Geology, Geological Survey of Canada, Contract 23294-7-0567/01-SG. C.A. Zelt was supported by a Natural Sciences and Engineering Research Council of Canada Postgraduate Scholarship.

number of simple features have been incorporated into the routine to expand its flexibility and range of applicability. These features include *S*-wave propagation and converted phases, approximate attenuation, head waves, and a reverse ray-direction amplitude calculation suitable for the interpretation of common-receiver profiles.

Velocity Model Parameterization

Ray-tracing algorithms are most strongly characterized by their velocity model parameterization. The degree of accuracy, practicality and efficiency of a particular routine is ultimately linked to the parameterization, with some degree of compromise between these three key attributes. The velocity model of the routine presented here can be described as a simple, layered, large-block, two-dimensional parameterization. In addition, the medium is assumed to be isotropic with lateral homogeneity in a direction normal to the plane of the model. The model is composed of a sequence of quasi-horizontal layers, the layers separated by boundaries which must cross the model from left to right without crossing another boundary. Each boundary is defined by an arbitrary number of points connected by straight-line segments of arbitrary dip.

Within each layer, the *P*-wave velocity structure is defined by specifying a single upper and lower layer velocity for each straight-line segment of the upper layer boundary. The upper and lower velocity pair may vary laterally within the layer (e.g., Figure 6a). Vertical boundaries separate each layer into large blocks and the emplacement of these boundaries is performed automatically by the routine as a requirement of the model parameterization. Vertical boundaries are necessary at each of the following points within a layer: (1) changes in slope of the line segments of the upper layer boundary, (2) changes in slope of the line segments of the lower layer boundary, and (3) changes in the upper or lower velocity within the layer. As a result of the vertical boundaries, each layer is broken up laterally into a series of large trapezoidal blocks with vertical left and right sides and upper and lower boundaries of arbitrary dip (Figure 1).

The velocity at a point within a trapezoid is determined by linear interpolation between the upper and lower velocity along a vertical path. For a trapezoid bounded above and below by line segments whose equations in the *x*-*z* plane are

$$z = m_1 x + b_1 \text{ and } z = m_2 x + b_2,$$

the *P*-wave velocity, v_0, at the point (x_0, z_0) within the trapezoid is given by

$$v_0 = [(v_1 m_2 - v_2 m_1)x_0 + (v_2 - v_1)z_0 + (v_1 b_2 - v_2 b_1)]/[(m_2 - m_1)x_0 + (b_2 - b_1)] \quad (1)$$

where v_1 and v_2 are the upper and lower velocities, respectively, within the trapezoid (Figure 1). The *S*-wave velocity is obtained from the *P*-wave velocity given in equation (1) using an assigned Poisson's ratio which may vary throughout the model but is constant within each trapezoidal block.

There are a number of advantages to having a large-block, trapezoidal model parameterization with constant velocities along the upper and lower boundaries: (1) a wedge-shaped structure with a vertical and horizontal velocity gradient can be modelled, (2) velocity discontinuities across layer boundaries can be readily incorporated into the model, (3) layer boundaries can be modelled as horizontal, dipping, or with considerable topographic relief through an appropriate combination of straight-line segments, (4) layers whose boundaries have considerable

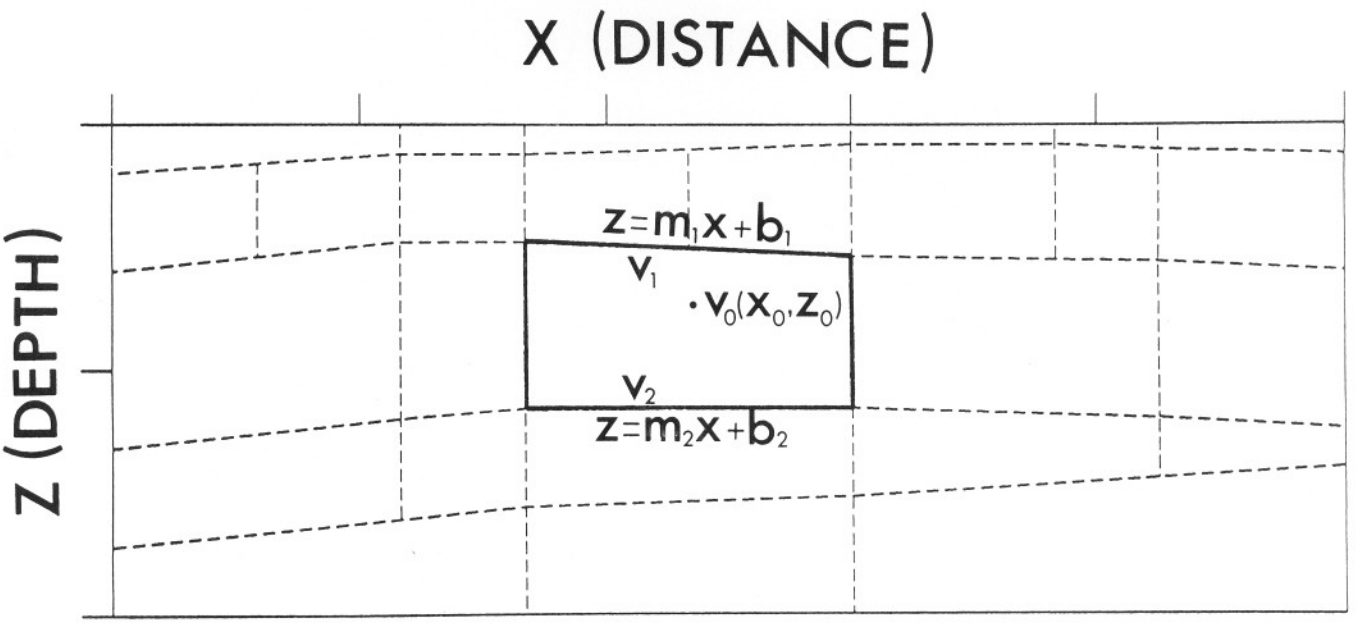

Fig. 1. An example velocity model consisting of 5 layers and 27 trapezoidal blocks. The velocity, v_0, at the point (x_0, z_0) is given by equation (1).

topographic structure can be assigned a single constant velocity along the full extent of the upper and/or lower boundary, (5) a trapezoid can be of sufficiently general shape so that a minimum number are required to represent typical earth models, and, therefore, the trapezoids will, on average, be large blocks within the model, and (6) the layered, large-block character of the model results in a nonuniform but consistent grid so that the position of a single boundary point can be adjusted and the velocity model remains consistent.

The algorithm allows for layers to shrink to zero thickness so that pinch-outs or isolated bodies can be considered. However, within a trapezoid adjacent to the pinch-out at the point where the layer thickness shrinks to zero, the velocity will be undefined if the upper and lower velocities within the trapezoid are unequal. To avoid an undefined velocity, an equal upper and lower velocity within the adjacent trapezoid is specified.

Ray Tracing

To trace rays through the velocity model, the ray-tracing equations are solved numerically (cf. Červený et al., 1977; McMechan and Mooney, 1980). The two-dimensional ray-tracing equations solved by the routine are a pair of first-order ordinary differential equations; there are two sets:

$$\frac{dz}{dx} = \cot\theta \qquad \frac{dx}{dz} = \tan\theta$$

$$\frac{d\theta}{dx} = \frac{(v_z - v_x \cot\theta)}{v} \quad (2a) \qquad \frac{d\theta}{dz} = \frac{(v_z \tan\theta - v_x)}{v} \quad (2b)$$

with initial conditions

$$x = x_0,\ z = z_0,\ \theta = \theta_0$$

[Červený et al., 1977, equations 3.19 and 3.19′]. The variable θ is the angle between the tangent to the ray and the z-axis, v is velocity, and v_x and v_z are partial derivatives of velocity with respect to x and z, respectively. The point (x_0, z_0) is the source location and θ_0 is the ray take-off angle. To ensure stability, system (2a) is solved with x as the integration variable when the raypath is near-horizontal, and system (2b) is solved with z as the integration variable when the raypath is near-vertical. To solve either system, the routine uses the Runge-Kutta method (Sheriff and Geldart, 1983, pp. 157-158) with error control as suggested by Červený et al. (1977). To complete the ray-tracing algorithm, Snell's law must be satisfied at each point of intersection of a ray with a model boundary.

The ray step length, Δ, used in solving system (2a) or (2b) is an increment in either the x or z direction, respectively, and is given by the relationship

$$\Delta = \frac{\alpha v}{|v_x| + |v_z|} \quad (3)$$

where α is a user-specified constant which will be discussed further with reference to the examples. An examination of equation (3) reveals the following: if the local derivative of the velocity field is large, the corresponding step length will be small, and vice versa. This approach is based on the realization that strong ray bending will occur if the ray is under the influence of a strong velocity gradient, whereas raypaths are essentially straight lines if the local velocity gradient is near zero. Thus, equation (3) is used to adjust the ray step length at each point so as to maximize efficiency while maintaining accuracy by avoiding unnecessarily small step lengths when the ray bending is small and the potential inaccuracy due to the use of a large step length when the ray bending is large. If the velocity within a trapezoid is constant, no ray bending occurs, the raypath is calculated analytically and the numerical solution of system (2a) or (2b) is avoided. Since the velocity, given by equation (1), and its partial derivatives are analytic functions of position, systems (2a) and (2b) can, in conjunction with equation (3), be solved efficiently.

Once a ray has been traced through the model, it is defined by a series of points, the spacing and number of points being dependent on the value of α used in equation (3). The total traveltime at the ray endpoint is then evaluated by simple numerical integration along the raypath using the trapezoidal rule.

Rapid forward modelling is accomplished through the routine's ability to search for the take-off angles of specific kinematic ray families. For a specific model layer, three types of ray families can be searched for: (1) rays which turn (refract) within the layer, (2) rays which reflect off the bottom of the layer, and (3) the ray which generates head waves along the bottom of the layer (Figure 2). For a turning ray family, the search mode seeks the take-off angles of the shallowest and deepest rays to turn within the layer. Once the take-off angles of these two rays have been determined within a prespecified distance, or a maximum allowable number of rays have been traced in the search mode, the entire ray family consisting of a specified number of rays with take-off angles between the shallow- and deep-ray take-off angles is traced. For a reflected ray family, the search mode seeks the take-off angle of the ray with the smallest take-off angle (measured from the horizontal) which reflects off the bottom of the specified model layer. Once this take-off angle is appropriately determined, the complete family consisting of a specified number of rays with take-off angles between the smallest reflected take-off angle and a prespecified maximum take-off angle, typically near 90°, is traced. In order to generate head waves along a layer boundary, the search mode seeks the ray which intersects the bottom of the layer at a critical angle, within a prespecified tolerance (cf. Whittall and Clowes, 1979). To trace the complete head-wave family, rays emerging at the critical angle are traced upward from the layer boundary and at a spacing specified by the user. In an analogous manner, a general diffracted ray family, in which the rays traced upward from the layer boundary

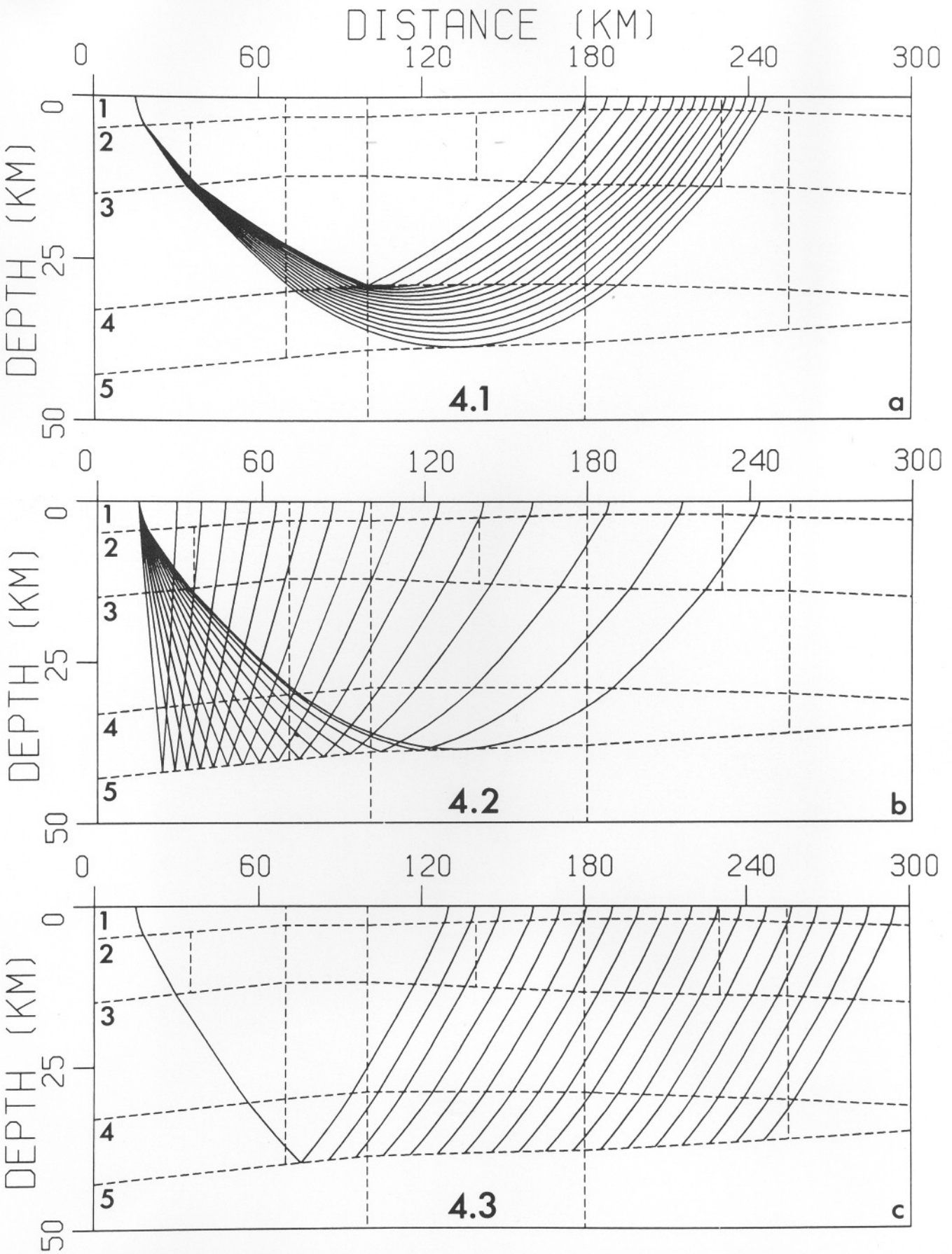

Fig. 2. Example of the three simplest kinematic ray families for a single layer (layer 4) of a 5-layer model. **(a)** Turning rays (ray code 4.1); **(b)** reflected rays (ray code 4.2); **(c)** head waves (ray code 4.3).

emerge at the angle of incidence of the generating ray, may be traced. This family may be used, for example, to model the kinematics of diffractions which travel along the top of a low-velocity layer and occur as first arrivals within the geometrical shadow. The generating ray in this case is the first ray of the reflected ray family in the layer above the low-velocity zone.

The manner in which the search mode operates in its search for any one of the four basic ray types is similar, so that only one will be considered in detail. Consider the case of determining the take-off angle of the shallowest ray to turn within a specified layer. If the medium were laterally homogeneous, this take-off angle, ϕ_0, measured from the horizontal in degrees, would be given by

$$\phi_0 = 90° - \sin^{-1}(v_0/v) \tag{4}$$

where v_0 is the velocity at the source and v is the velocity at the top of the specified layer. This take-off angle is used as a starting value in the search mode where v is the velocity at the top of the layer directly beneath the source. If the value of v is not the maximum velocity between the source and the top of the layer along a vertical path directly beneath the source, the value of v in equation (4) is replaced by this maximum velocity. If all velocities between the source and the top of the layer are less than or equal to the velocity at the source, a prespecified minimum take-off angle is used as the initial take-off angle in the search mode.

An initial ray with a take-off angle ϕ_0 is traced to its turning or reflection point. Within the search mode, rays are generally traced only to their turning or reflection points. However, if the model is strongly two-dimensional, it may in some cases be necessary to trace rays to their completion in order to determine correctly the appropriate take-off angles; a switch allows the user to select this option. A second ray is traced with a take-off angle of $\phi_0 + \delta\phi$ if the initial ray did not enter the layer specified, or $\phi_0 - \delta\phi$ if the ray entered the layer. The quantity $\delta\phi$ is a prespecified fraction of the quantity $|\phi'_0 - \phi_0|$ where ϕ'_0 is the initial take-off angle used in the search for the deepest turning ray in the layer. A third ray will be traced with a take-off angle of $\phi_0 \pm 2\delta\phi$ if both of the first two rays either did not enter the layer (+) or did enter the layer (–), or $\phi_0 \pm {}^1/_2\delta\phi$ if the first ray did not enter the layer, but the second did (+) or vice versa (–). Thus, when two raypaths bracket the upper layer boundary, a bisection of angles begins, but until this point the take-off angles are incremented by $\delta\phi$ (Figure 3).

The maximum number of rays traced in the search mode is specified by the user but will be terminated before this number if the distance between the endpoints of two successive rays is less than a prespecified distance. Typically, ten rays are sufficient to define accurately a specific take-off angle; however, for strongly two-dimensional models, twenty or more rays may be necessary. The search routine has been found through experimentation to work successfully and efficiently for models with strong lateral variations. Take-off angles can also be supplied manually by the user.

The three basic kinematic ray families obtained by the search mode can each be modified through simple numerical codes and switches to include any number or combination of multiple reflections, free-surface reflections, and *P-S* or *S-P* conversions at any layer boundary. There is no restriction on the location of shotpoints within the model. Rays from multiple shots may be traced in a single run so that the corresponding fit of the theoretical to observed data can be monitored simultaneously for all

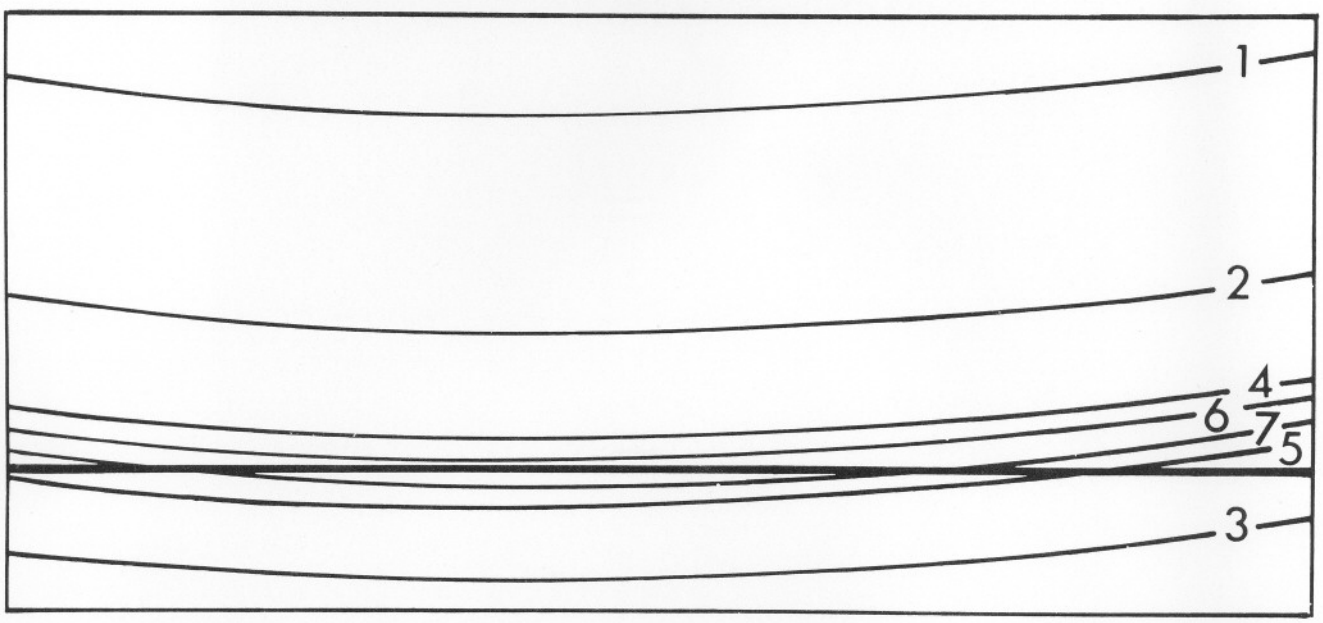

Fig. 3. The first seven rays traced in a hypothetical search for the shallowest ray to turn in the lower layer. The solid line is the model boundary separating the upper and lower layer.

shotpoints along a particular line. For shotpoints located below the model surface, rays may also be traced upwards. Receiver locations are assumed to be at the top of the model.

The search routine is based on the determination of ray families composed of kinematically similar rays, as opposed to two-point ray tracing in which rays are traced to specific receiver locations (cf. Cassell, 1982). A ray-family search is a superior approach when forward modelling since a particular region of interest within the model can be examined through specification of the appropriate ray families. Therefore, when constructing a velocity model, the interpreter can begin model construction at the earth's surface and proceed downwards, matching arrivals from progressively deeper layers within the earth. The traveltime (and amplitude) associated with an arbitrary point on the earth's surface are determined by linearly interpolating across the endpoints of the two closest rays which bracket the point of interest. For models with strong lateral variations, it may be necessary to trace relatively more rays in order to obtain accurate interpolated traveltimes and amplitudes.

Amplitude Calculations

The complex amplitude of turning and reflected rays, possibly multiply reflected and/or converted, is calculated by zero-order asymptotic ray theory [Červený et al., 1977, equation (2.56)] as given by the expression

$$A = A_0 q(-1)^{\varepsilon}/L \tag{5}$$

where A is the amplitude of the ray at its endpoint, A_0 is the initial ray amplitude, q is a factor which accounts for the energy partitioning at model boundaries, and L is the geometrical spreading. The factor ε is equal to the number of times the direction of positive displacement changes along *SV* segments of the raypath with respect to the ray-coordinate system (Červený and Ravindra, 1971, pp. 72-73). A point source with uniform directional characteristics is assumed.

The initial ray amplitude is set equal to unity so that the amplitude, A, is a relative amplitude; however, the ratio of *SV*- to *P*-wave energy generated by the source can be specified. The quantity q is given [Červený et al., 1977, equation (2.58)] by:

$$q = \left(\frac{v_0 \rho_0}{v_r \rho_r} \right)^{\frac{1}{2}} \prod_{i=1}^{n} \left(\frac{v'_i \rho'_i}{v_i \rho_i} \right)^{\frac{1}{2}} Z_i \tag{6}$$

where:

n = number of model boundaries encountered by ray;

v_0, ρ_0 = velocity and density at the source whose product is impedance;

$v_r\rho_r$ = impedance at the receiver;

$v_i\rho_i$ = impedance at the point of incidence at the ith boundary;

$v'_i\rho'_i$ = impedance at the point of emergence at the ith boundary;

Z_i = Zoeppritz displacement-amplitude coefficient at the ith boundary.

The relationship between density, ρ, and *P*-wave velocity, v_p, can be specified in two ways:

$$\rho = 0.252 + 0.3788 v_p; \qquad \rho = 1.732\, v_p^{\frac{1}{4}}$$

(Birch, 1964; Gardner et al., 1974). The complex Zoeppritz displacement-amplitude coefficients for incident *P*- and *SV*-waves are calculated using a routine based on that described by Young and Braile (1976) which allows for the calculation of surface reflection coefficients, but has been modified to allow for the calculation of surface conversion coefficients of vertical- and horizontal-component type for incident *P*- and *S*-type rays [Červený and Ravindra, 1971, equations (2.89) and (2.90)].

The geometrical spreading is given by

$$L = \left(L_{\perp} L_{\parallel} \right)^{\frac{1}{2}} \prod_{i=1}^{n} \left(\frac{\cos\theta_i}{\cos\theta'_i} \right)^{\frac{1}{2}}$$

where $L_{\perp}$ is the out-of-plane spreading, $L_{||}$ is the in-plane spreading, and the product term represents a compensation for the discontinuity in the spreading functions across model boundaries (Červený et al., 1977, p.38). The angles θ_i and θ'_i are taken at the point of incidence and emergence at the ray's intersection with the ith model boundary. The out-of-plane spreading can be expressed as

$$L_{\perp} = \frac{1}{v_0} \int v \, \mathrm{d}\, l \tag{7}$$

where l is the raypath length [Červený and Hron, 1980; Červený, 1981, equation (31)]. The integral in equation (7) is evaluated using the trapezoidal rule. The in-plane spreading is given by

$$L_{\parallel} = \cos\theta_r \frac{\delta r}{\delta \theta_0} \tag{8}$$

where θ_r is the angle between the vertical and the raypath at the receiver, r is the distance between the source and receiver (range), and θ_0 is the angle between the vertical and the raypath at the source (take-off angle) [Červený et al., 1977, equation (3.69)]. The evaluation of the derivative in equation (8) can be made through an examination of the kinematics of a set of similar rays. The approach used is most like that used by Marks (1980). To evaluate the derivative, a separate cubic spline is fit to each prograde and retrograde segment of the curve defined by range versus take-off angle for all rays of the same kinematic family and the derivative for each ray in the family can be obtained directly from the splines. The advantage of this approach is that additional rays, beyond those already traced for the family, do not have to be traced, as

is necessary with other routines. A limitation is that for strongly two-dimensional models, the slope of the cubic spline may be sensitive to the number of rays which constitute the family. The greater the lateral inhomogeneity of the model, the greater the number of rays which must be traced in order to fully sample all aspects of the lateral variation of the model. For most models which have been studied, 10 to 20 rays per family were sufficient.

For the interpretation of common-receiver profiles, often encountered in marine OBS studies, it is necessary to calculate amplitudes in the reverse direction to which rays are traced. A reverse-ray-direction amplitude calculation is accomplished by switching the source and receiver quantities and incident and emergent quantities in equation (6) and adjusting the geometrical spreading by a factor dependent on the source and receiver velocities [(Richards, 1971, equation (18)]. These adjustments are made since the reciprocity of amplitudes is not necessarily preserved by the approximations of ray theory (Razavy and Lenoach, 1986). In addition, the surface conversion coefficient must be calculated at the ray source.

In most practical situations, the modelling of head waves is not required as turning rays in the lower medium dominate. However, in some instances topographic structure on a layer boundary can result in a shadow zone with respect to turning rays in the lower medium. In this case, head waves will represent the first arrivals at certain receiver locations. The routine allows for the calculation of *P* and *SV* head-wave amplitudes through first-order asymptotic ray theory assuming the layer, along the top of which the wave propagates, has zero velocity gradient. At present, the routine requires that the raypaths toward and away from the head-wave boundary do not contain reflection or conversion points.

The calculation of head-wave amplitudes is made in the same manner as that of Spence et al. (1984); however, no explicit reparameterization of the velocity model into a series of thin homogeneous layers is required since the region between each point defining the raypath toward and away from the head-wave boundary can be considered a homogeneous layer if the average velocity between points is used as the layer velocity. The head-wave amplitude, A^H, is given by [Červený and Ravindra, 1971, equations (5.22) and (5.29)]:

$$A^H = \frac{\bar{v}\,\Gamma_k \tan\theta'_k}{i\omega l^{\frac{3}{2}} (v_k \bar{v})^{\frac{1}{2}} L_\perp^H L_{\|}^H} \prod_{\substack{i=1 \\ i \neq k}}^{N-1} Z_i \qquad (9)$$

where

$$L_\perp^H = \left(l \frac{\bar{v}}{v_1} + \sum_{i=1}^{N} \frac{l_i v_i}{v_1} \right)^{\frac{1}{2}}; \quad L_{\|}^H = \left(\frac{v_k}{v_1} \right)^{\frac{1}{2}} \prod_{i=1}^{k-1} \frac{\cos\theta_i}{\cos\theta'_i};$$

N = number of line segments comprising the complete head-wave raypath;

θ_i, θ'_i = angle of incidence and emergence at the ith boundary;

v_i = velocity along the ith ray segment;

l_i = length of ith ray segment;

k = head-wave boundary number;

v = velocity below head-wave boundary;

l = length of raypath along head-wave boundary;

ω = dominant frequency of head waves;

Γ_k = head-wave coefficient (Červený and Ravindra, 1971, pp. 108-109).

The Zoeppritz routine has been modified to include the computation of the head-wave coefficient. If the velocity below the head-wave boundary varies laterally, the value of v is set equal to the appropriate average value. At the critical point, the value of l equals zero so that the corresponding ray amplitude is undefined. To avoid this problem, an ad-hoc approach used by Spence (1983) is incorporated which assures that the value of l used in equation (9) remains greater than a prespecified minimum value. Therefore, the head-wave amplitude within the zone of interference with the reflected ray is not valid. At present the routine does not allow for the calculation of amplitudes for the general diffracted-ray family described earlier; however, this would be possible if an angle-dependent diffraction coefficient were incorporated into a formula similar to equation (9).

The effect on amplitudes due to attenuation can be considered in an efficient manner by the routine through a major simplifying assumption: the attenuation is independent of frequency. For each ray traced, the attenuation is calculated at a specified dominant frequency and this attenuation is applied equally at all frequencies. This results in the incorporation of a single multiplicative scale factor into equations (5) and (9) so that the coupled phenomenon of dispersion is neglected. The scale factor, A_Q, is given by (Aki and Richards, 1980, pp. 168-169):

$$A_Q = \prod_{i=1}^{N} \exp\left[-\omega l_i / 2 v_i Q_i \right]$$

where:

N = number of line segments comprising the complete raypath;

ω = dominant frequency;

l_i = length of the ith ray segment;

v_i = average velocity along the ith ray segment;

Q_i = Q-attenuation value along ith ray segment.

This approximate method can be expected to be a good approximation to a more accurate frequency-dependent calculation if the source energy is assumed to be concentrated within a narrow frequency band or the attenuation is not large. *P*- and *S*-wave Q values can be assigned to each model block.

Once the amplitude calculations for all rays which reached the model surface are complete, synthetic seismograms for a set of specified surface locations can be

generated. The approach used is similar to that used by McMechan and Mooney (1980) and Spence et al. (1984). The time and complex amplitude of all arrivals on a particular seismogram are obtained by linearly interpolating across the endpoints of the two closest rays which bracket the seismogram location and are of the same kinematic ray type. A superposition of all arrivals on the seismogram results in a trace consisting of a series of impulses, each with appropriate amplitude and phase shift. The final seismogram is obtained through a convolution with an apparent source function.

Examples

The routine presented in this paper is based on the ray method and as such the accuracy and limitations of its dynamic calculations are similar to all other ray-tracing routines. For a thorough discussion of the limitations of the ray method and its comparison to other more accurate methods, the reader is referred to Červený (1985). The following examples are not intended to show the weaknesses of the ray method, but rather the positive aspects of the new routine as a practical forward-modelling algorithm. All computations were performed on a 12-Mips Amdahl 5860 computer.

Efficiency and accuracy

The first example illustrates the routine's efficiency and accuracy as compared to the algorithm of Spence et al. (1984), an extension of the Whittall and Clowes (1979) ray tracer in which the model is parameterized in terms of large polygonal blocks within which the velocity gradient vector is constant. Since the Spence et al. algorithm uses analytic expressions to trace rays and calculate traveltimes, these quantities may be considered to be exact with respect to ray theory. Therefore, a comparison of these values with the new routine's will reveal the degree of inaccuracy associated with solving the ray tracing and traveltime equations numerically. As a check on the routine's amplitude calculations, numerous models were tested and the results showed close agreement with those obtained from the Spence et al. algorithm. Due to the manner in which the new routine and that of Spence et al. parameterize velocity models, only models in which the boundaries are horizontal or vertical can be compared.

The model chosen for the comparison study is a generalized earth model consisting of three layers (Figure 4a). The three layers represent sediment, crust and upper mantle and the velocity structure within each layer has been broken up laterally into six blocks. Two different numerical tests were made with this model: a study of the trade-off between CPU time and rms traveltime error, measured against the Spence et al. algorithm, as a function of ray step length; and a comparison of the CPU time required for a number of different types of runs of the two routines. In all cases, a total of 100 rays were traced through the model — 25 turning rays in each layer and 25 rays reflected off the crust-mantle boundary. For some runs of the new routine, additional rays were traced in the search mode to demonstrate the extra CPU time required. Figure 4b shows the 100 rays traced through the model by the new routine; and the corresponding traveltime curves and synthetic section are shown in Figures 4c and 4d.

Figure 5 shows the trade-off between accuracy and CPU time. The value of the step-length parameter, α,

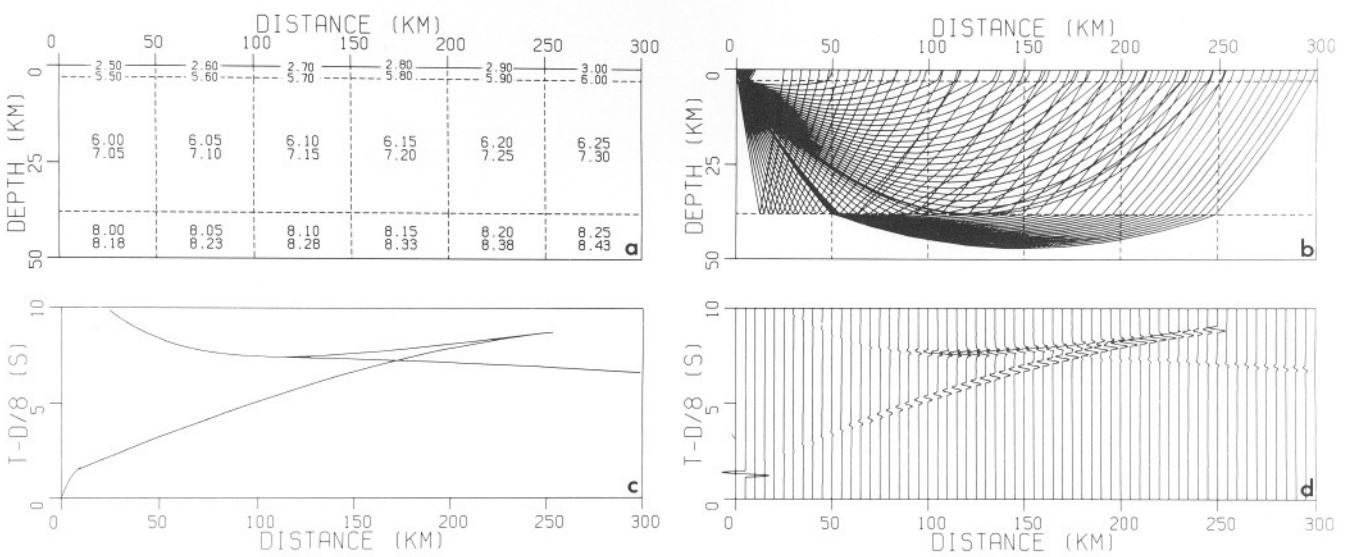

Fig. 4. Example in which the efficiency and accuracy of the new routine is studied. **(a)** Velocity model consisting of three layers with six blocks in each layer. The upper and lower velocity in km/s is indicated within each model block. **(b)** One reflected and three turning ray families traced through the model. **(c)** Reduced traveltime curves corresponding to the rays traced in (b). **(d)** Synthetic section corresponding to the rays traced in (b). The source wavelet is a single-cycle sine wave. The trace amplitudes have been scaled by a factor proportional to distance.

used in equation (3) was varied between 0.4 and 0.0075. In all runs, amplitudes were not calculated and no plots were generated. Also, a maximum of 20 additional rays were traced in the search mode to define the take-off angles of each ray family.

One might expect the CPU time to increase monotonically and the rms error to decrease monotonically as the value of α decreases. This is the general trend observed; however, a minimum CPU time occurs at $\alpha = 0.15$ and a minimum rms error occurs at $\alpha = 0.015$. The CPU time minimum is due to two factors. First, regardless of the value of α used, a constant single-step tolerance is used in the Runge-Kutta routine. Therefore, for relatively large step lengths, the number of subintervals required by the Runge-Kutta routine may become large. Second, the search mode does not operate effectively when too large a value of α is used. This results in relatively more rays traced in the search mode. The minimum in rms travel-time error is also due to two factors. The fixed single-step tolerance used in the Runge-Kutta routine does not allow for increased accuracy when relatively small step lengths are used. Also, the accumulated round-off error of this single precision routine prevents increased accuracy with decreased step length.

Figure 5 shows that the CPU time increases by a factor of about five for a corresponding decrease in the value of α of about fifty. The variations in the rms traveltime error are perhaps more important and should be considered when selecting an appropriate value of α. Typically, crustal refraction data will have a traveltime measurement uncertainty of between 10 and 20 ms. Therefore, a value of α less than about 0.15 should be sufficient in

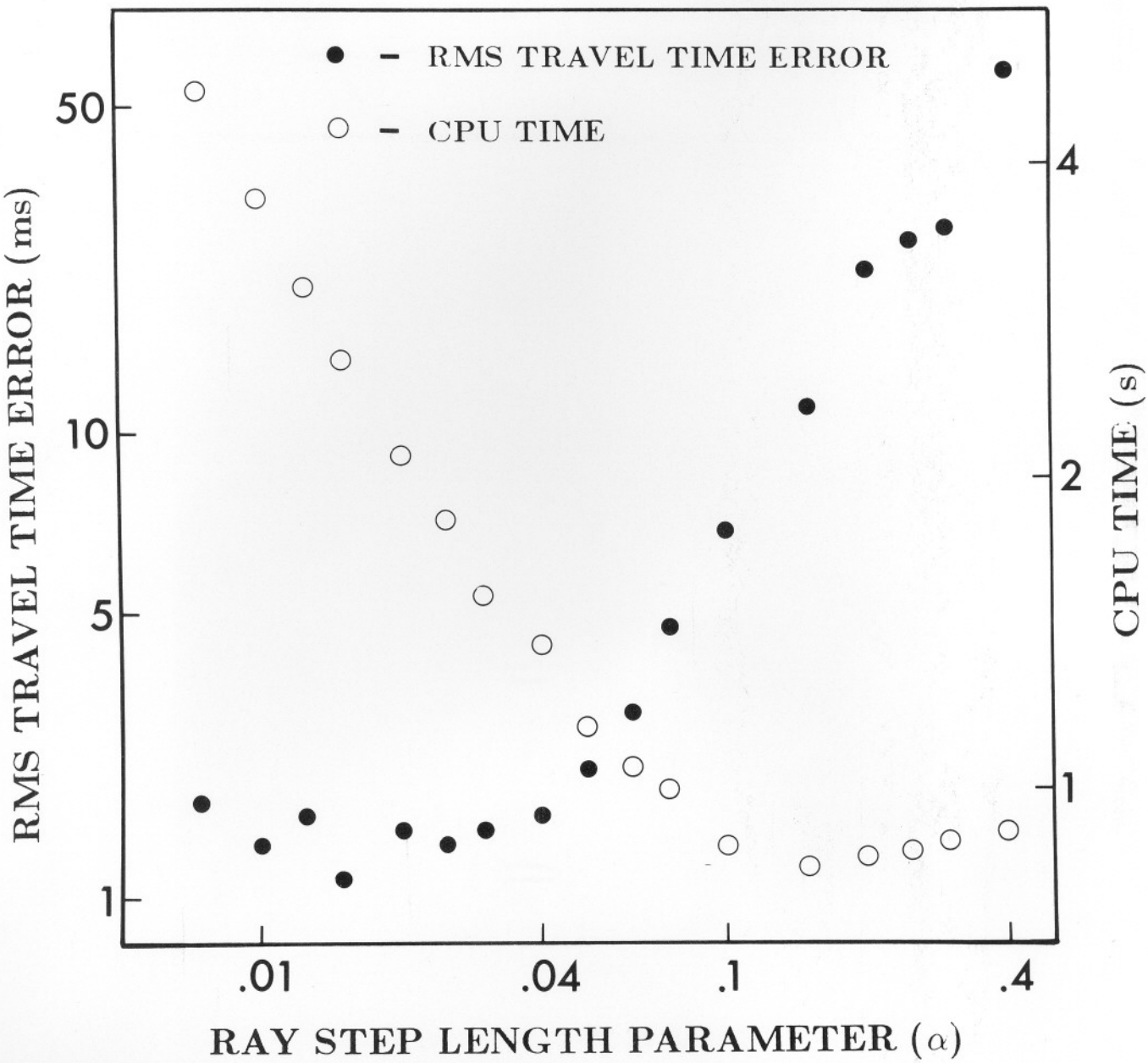

Fig. 5. Trade-off between accuracy and CPU time as a function of the ray step-length parameter, α, used in equation (3).

most cases (Figure 5). Also, values of α less than about 0.05 increase the CPU time required without significantly improving accuracy. Finally, the CPU time and rms error minimums suggest that for this model, and probably all models that are normally considered, the value of α should be between 0.015 and 0.15.

The number of points defining rays increases as the value of α decreases. For this example, the ray defined by the greatest number of points was, in each run, the deepest turning ray in the second layer. For α = 0.4, 0.1, 0.03 and 0.01, the number of points defining this ray was 13, 33, 94 and 267, respectively.

The second test done with the model shown in Figure 4a was a comparison of the CPU time required for the new routine with that of Spence et al. (1984). Table 1 summarizes the results of eleven runs. For all runs of the new routine, α was equal to 0.1. For the first five runs listed in Table 1, the take-off angles for the new routine were supplied manually. For the last six runs the take-off angles for the new routine were determined through the search mode with the maximum number of rays traced to define each take-off angle equal to 10, 25 or 50. The total additional number of rays traced in each case was 55, 77 and 102, respectively. For all runs, the take-off angles for the Spence et al. routine were supplied manually.

Description of Run‡	CPU Time (Spence et al.) (s)	CPU Time (This Paper) (s)		
1	0.70	0.65		
1,2	1.24	0.74		
1,3	1.07	0.81		
1,2,3	1.50	0.94		
1,2,3,4	6.08	2.04		
1,3,5	1.07	0.97	1.02	1.08
1,2,3,5	1.50	1.05	1.10	1.14

Table 1. CPU-time comparison for model and rays traced as shown in Figure 4 on 12-MIPS Amdahl 5860 computer.
‡1 — calculate raypaths and traveltimes; 2 — calculate amplitudes; 3 — generate plot of rays and traveltime curves; 4 — calculate synthetic section and generate plot; 5 — search mode for new routine with maximum number of rays traced to define each take-off angle equal to 10, 25 and 50.

Table 1 shows that the new routine required less CPU time for all runs except one in which the search mode was used and amplitudes not calculated. There are three reasons for the new routine's favourable comparison. First, the new routine operates in single precision whereas the Spence et al. routine requires double precision because of the way in which traveltimes and the in-plane geometrical spreading are calculated. Second, the manner in which the next block is determined when a ray intersects a model boundary is generally more efficient in the case of the new routine due to its layered, grid-like, model parameterization. Finally, to calculate the in-plane spreading, the routine of Spence et al. traces a second ray for every ray traced in order to estimate the derivative in equation (8). The effect of this additional ray tracing is evident in the CPU times for the runs in which amplitudes are calculated. The relative efficiency of the new routine for the run in which the synthetic section was generated is due in part to the incorporation of a time/cost-saving feature in which zero-amplitude portions of traces are plotted as two points at either end connected by a straight line.

Even with the additional ray tracing in the search mode, the new routine generally required less CPU time. With the maximum number of rays traced to define each take-off angle equal to 10, the routine was able to define adequately the take-off angles of each of the corresponding ray families. Setting this maximum to 25 and 50 resulted in additional refining of the take-off angles.

Crustal refraction example

The second example is an application of the routine to the modelling of an observed crustal refraction data set. The complete data set consists of four reversed lines each approximately 300 km long from the Peace River Arch region (Ellis et al., 1986). Figure 6a shows the final block velocity model for a single line of the experiment in which profiles from shots at 0 and 270 km model distances were interpreted through a comparison of observed and theoretical traveltimes and amplitudes (Zelt and Ellis, 1988). Figure 6b is a smoothed isovelocity contour representation of the model and shows more clearly that the model possesses significant lateral variations. The model consists of 9 layers — 2 sedimentary, 5 crustal and 2 upper-mantle — and 51 blocks.

Figure 7a shows the complete set of all rays traced through the model from the shot point at 270 km. A total of fourteen ray families consisting of 150 rays were traced. An additional 252 rays were traced in the search mode. The ray families include turning rays in each layer and reflections off the four intracrustal boundaries, the crust-mantle boundary, and an upper mantle boundary at a depth of about 56 km. The corresponding traveltime curves are shown in Figure 7b compared with the observed traveltime picks. The synthetic record section is shown in Figure 7c. With a value of α = 0.1, the total CPU time required to calculate and plot all rays, traveltime curves, and the synthetic section was 4.26 s. The corresponding observed record section is shown in Figure 7d. The agreement between the synthetic and observed data is generally good; however, the relatively high amplitudes of the intracrustal reflected phases have not been reproduced by the model. Strong reflections of this type have been explained (e.g., Fuchs, 1969; Valasek et al., 1987; Christensen and Szymanski, 1988) as a result of constructive interference associated with a layered transition zone due to variations in composition, texture and anisotropy or other physical properties. A zone of this type cannot be modelled using ray theory.

A brief description of the general modelling procedure used to arrive at the final model shown in Figure 6 is

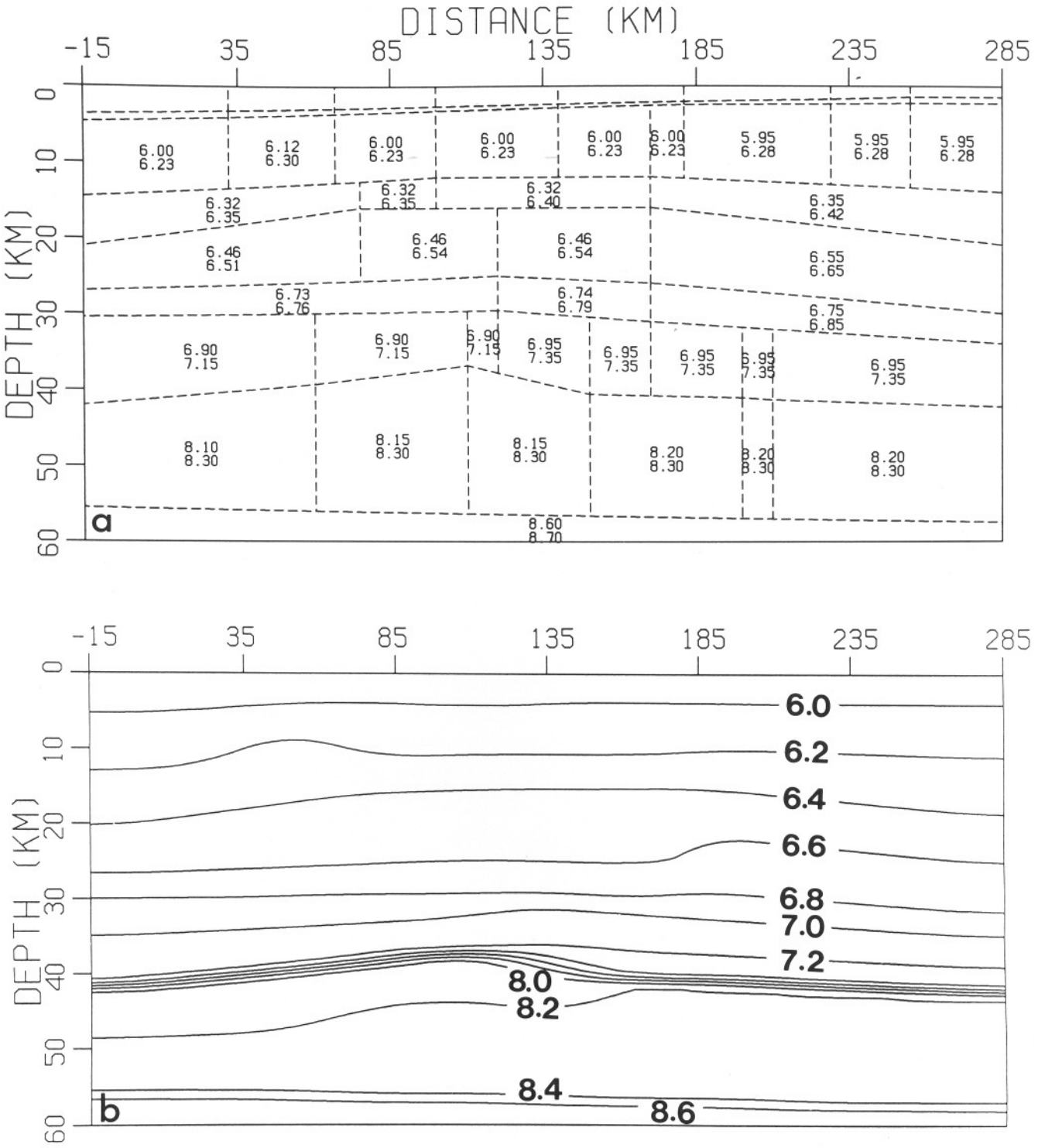

Fig. 6. Velocity model interpreted for a real, reversed, crustal refraction data set — PRASE, Line C (Ellis et al., 1986). **(a)** Block model representation in which the upper and lower velocity in km/s is indicated within each trapezoid. The surface velocity in the first sedimentary layer varies from 4.25 to 1.75 km/s from left to right and the lower velocity in the second sedimentary layer varies from 6.0 to 4.0 km/s from left to right. **(b)** A smoothed, isovelocity contour representation of the velocity model. The velocities of contours are indicated in km/s.

instructional. First, eight sonic logs from wells close to the line were analyzed to obtain a two-layer sediment-velocity model. The subbasement crustal and upper mantle starting velocity model was obtained by connecting together the two best-fitting laterally homogeneous models which satisfied the traveltimes of the profiles from either shot. Through a trial-and-error scheme, this model was adjusted to match the traveltimes of arrivals for both shots from progressively deeper layers within the crust and upper mantle. Finally, a comparison of the initial synthetic section obtained from the best-fit traveltime model with the observed section showed that a few minor

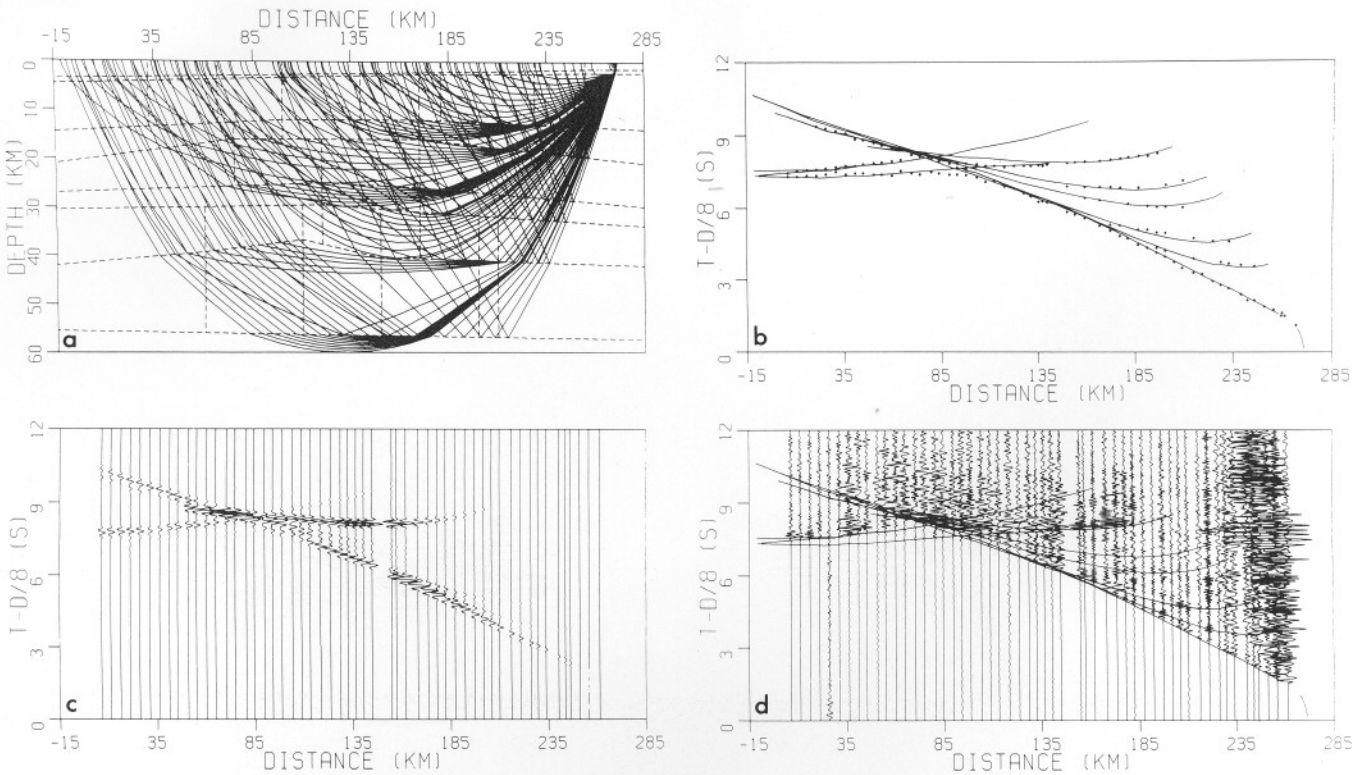

Fig. 7. Application of the new routine to the interpretation of a real crustal refraction data set — PRASE, Line C — Shot C2 (Ellis et al., 1986). **(a)** Rays traced through velocity model. **(b)** Comparison of the observed traveltime picks (symbols) and the calculated traveltime curves (lines). **(c)** Synthetic section corresponding to the rays traced in (a). The source wavelet is a low-passed Ricker wavelet. **(d)** Observed record section bandpass filtered from 2 to 12 Hz with calculated traveltime curves superimposed. The traces in (c) and (d) have been scaled by a factor proportional to distance.

adjustments were necessary to fit the amplitudes satisfactorily. The velocity gradients of some layers were adjusted to better match turning-ray amplitudes; and velocity contrasts across layer boundaries were adjusted to improve reflected ray amplitudes. This single sequence of steps resulted in the model presented in Figure 6. For a more complicated or strongly two-dimensional model, or for further refinement of a model, some or all of the above modelling steps may be repeated several times.

Complex crustal model

For the third example, a generalized crustal model of an oceanic-continental subduction zone is presented (Figure 8a). This model is a simplified version of that developed by Spence et al. (1985) of the subduction zone of western Canada. The purpose of this example is to illustrate the degree of lateral inhomogeneity possible with the model parameterization of the new routine. The layer pinch-out feature discussed earlier has allowed the obliquely dipping oceanic plate to be incorporated into the model. Five continental layers on the right side of the model have been pinched out above the subducting plate and four oceanic layers on the left side of the model have been pinched out at the bottom right of the model. Figure 8b shows turning and reflected rays traced through the subducting oceanic upper mantle and the corresponding synthetic section is shown in Figure 8c.

Exploration statics problem

The final example is an application of the routine to the study of the effects of near-surface velocity anomalies on CMP data, i.e., the statics problem. The routine was modified so that a collection of CMP gathers could be obtained in a single run. The model is presented in Figure 9a and consists of a horizontal reflector underlying a low-velocity layer of varying thickness. A common-shot gather and CMP gather for the same point in the model are shown in Figures 9b and 9c, respectively. The CMP gather after NMO correction is presented in Figure 9d. The misalignment of arrivals in Figure 9d is due primarily to the lateral variations in thickness of the upper layer, but is also due to the increase in velocity with depth within the model.

Discussion

This routine offers greater practicality than existing forward-modelling ray-tracing algorithms. In addition, the efficiency and range of model types which can be considered is comparable to current, widely used routines. Fundamental to the new routine is its simple, lay-

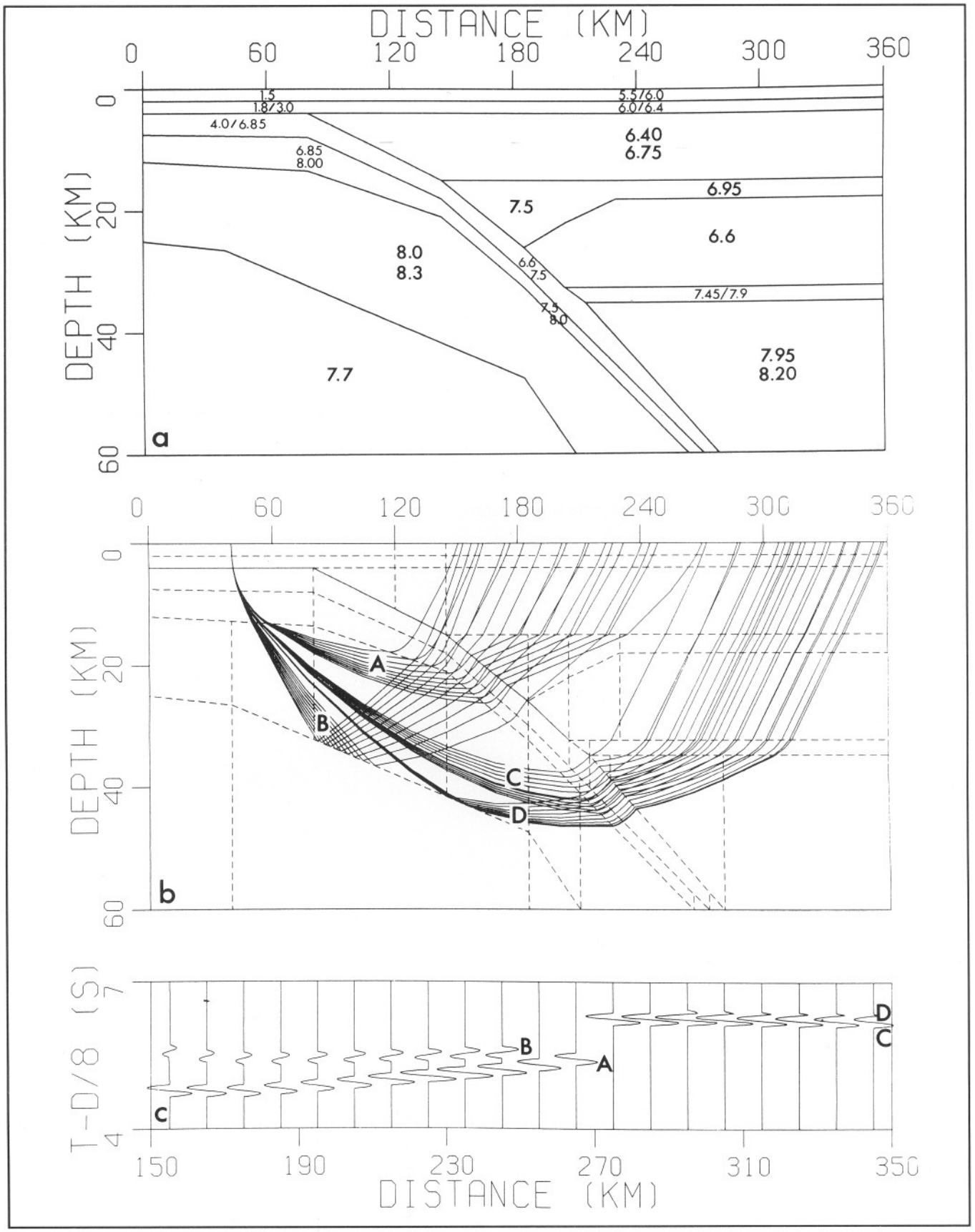

Fig. 8. Application of the new routine to a model with strong lateral inhomogeneity. **(a)** Velocity model with only layer boundaries shown. The velocities in km/s are indicated within each layer. **(b)** Some turning and reflected rays traced through the model. **(c)** Synthetic section corresponding to the rays traced in (b). The source wavelet is a single-cycle sine wave. The two turning ray families are identified in (b) and (c) by the letters A and C and the two reflected families by B and D.

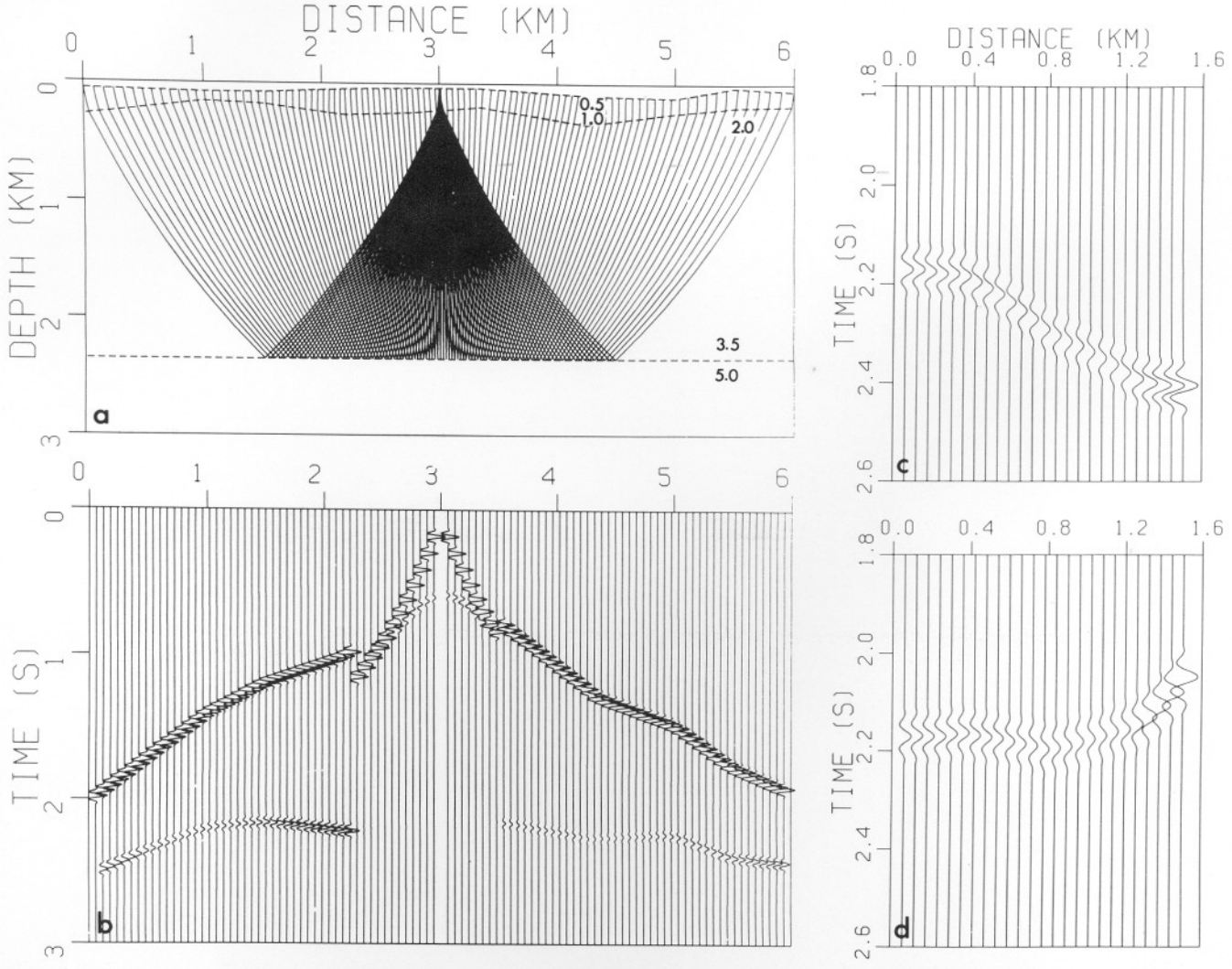

Fig. 9. Application of the routine to the study of the effects of near-surface velocity anomalies on CMP data. **(a)** Reflected rays in second layer traced through model. Upper and lower velocities in km/s are indicated within each layer. Vertical block boundaries are not shown. **(b)** Common-shot gather at 3 km model distance for turning and reflected rays traced through first two layers of model in (a). Each trace is scaled to a common maximum amplitude. **(c)** CMP gather at 3 km model distance. Only the reflected phase from second layer is included. **(d)** CMP gather in (c) after NMO correction using the rms velocity to the second layer reflector (2.38 km/s). Distance in (c) and (d) is half offset and the correct relative amplitude of each trace is presented.

ered, large-block velocity model parameterization. The layered nature of the model is valuable in that it allows the user to select specific layers within which, or layer boundaries at which, turning, reflection and conversion are to occur. The large-block parameterization is vital for efficiency since the velocity and its derivatives necessary for the solution of the ray-tracing equations are simple analytic functions of position and the number of model boundaries crossed by each ray is minimized. Another important advantage of large blocks is that the number of zero- and first-order discontinuities in velocity within the model can be minimized. This reduces the difficulties which can arise in the application of the ray method to *blocky* models, in particular, with regard to amplitude calculations [Cormier and Spudich, 1984, equations (4.1) to (4.3)]. The parameterization requires only a single upper and lower velocity to define the velocity field within each trapezoid and layer boundaries are a series of straight-line segments. This allows the user to alter the model easily and quickly so that the new velocity structure is always well-defined and predictable.

A number of relatively simple features incorporated into the algorithm, and which are often necessary in refraction interpretation, give the routine flexibility and a wide range of applicability. These features include layer pinch-outs, *S*-wave propagation and converted phases, multiple and surface reflections, approximate attenuation, head waves, no restriction on source location, multiple sources in a single run, and a reverse ray-direction amplitude calculation. The latter capability is necessary for the interpretation of marine data in which common-receiver profiles are involved.

As a practical algorithm for forward-modelling interpretation of crustal refraction data, the only significant limitation of the routine is that of the ray method itself. In particular, a blocky velocity structure can introduce false

highs and *lows* into amplitude calculations with respect to finite-frequency wave propagation due to discontinuities in velocity gradients at model boundaries. This problem is in addition to the fundamental inapplicability of the ray method in regions about caustics, critical points and geometrical shadows. The incorporation of Gaussian-beam amplitudes into the routine would be a straightforward procedure and would remove the above-mentioned difficulties associated with the dynamic properties of ray theory. However, this modification does not appear to be necessary or practical at this point, given the general quality of most refraction data sets and the somewhat unpredictable nature of Gaussian-beam seismograms (Müller, 1984; Červený, 1985). To reduce some of the artificial highs and lows associated with ray amplitudes, allowance within the routine is made for a specified amount of smoothing of the amplitude curves for each ray family. In addition, layer boundaries may also be smoothed so that the angle of incidence and reflection or transmission is calculated assuming the local slope of the smooth boundary. This *simulation* of smooth boundaries is simple and efficient to apply and can be important for raypaths which cross layer boundaries near a point at which the boundary consists of two line segments of differing slope.

The routine was developed for use in the interpretation of crustal refraction data; however, a number of other applications are possible — for instance, the CMP example presented earlier. The routine would also be suitable as a fast forward-modelling algorithm for iterative migration/inversion of reflection data. The appropriate conversion of coding would be straightforward to allow for the routine's implementation on a microcomputer, as was done for the Spence et al. (1984) algorithm (Crossley, 1987).

A possible alternate model parameterization could be implemented in which the velocity field within each trapezoid is defined by velocity values specified at each of the four corners of the block. This would allow the velocity structure within a layer to be free of velocity discontinuities at vertical block boundaries and the parameterization would require only a single additional upper and lower velocity pair to be specified for each layer. It may be possible to improve the efficiency of the routine by automatically breaking each trapezoid into two or more triangular blocks within which the velocity gradient is a constant (Chapman and Drummond, 1982; Müller, 1984). However, this would at least double the number of blocks within the model and result in each ray crossing about twice as many model boundaries. This may reduce the efficiency and degrade the amplitude calculations further due to the increased number of discontinuities in velocity gradient.

References

Aki, K. and Richards, P.G., 1980, Quantitative seismology: W.H. Freeman & Co.

Birch, F., 1964, Density and composition of mantle and core: J. Geophys. Res. **69**, 4377-4388.

Cassell, B.R., 1982, A method for calculating synthetic seismograms in laterally varying media: Geophys. J. Roy. Astr. Soc. **69**, 339-354.

Červený, V., 1981, Computation of geometrical spreading by dynamic ray tracing: Stanford Exploration Project, Rep. No. **28**, 49-60.

_____ , 1985, Gaussian beam synthetic seismograms: J. Geophys. **58**, 44-72.

_____ and Hron F., 1980, The ray series method and dynamic ray tracing system for three-dimensional inhomogeneous media: Bull. Seis. Soc. Am. **70**, 47-77.

_____ and Pšenčík, I., 1981, 2-D seismic ray package: Res. Rep., Inst. Geophys., Charles Univ. (Prague).

_____ and Ravindra, R., 1971, Theory of seismic head waves: Univ. of Toronto Press.

_____ , Molotkov, I. and Pšenčík, I., 1977, Ray method in seismology: Charles Univ. Press.

Chapman, C.H. and Drummond, R., 1982, Body-wave seismograms in inhomogeneous media using Maslov asymptotic theory: Bull. Seis. Soc. Am. **72**, S277-S317.

Christensen, N.I. and Szymanski, D.L., 1988, Origin of reflections from the Brevard fault zone: J. Geophys. Res. **93**, 1087-1102.

Cormier, V.F. and Spudich, P., 1984, Amplification of ground motion and waveform complexity in fault zones: Examples from the San Andreas and Calaveras Faults: Geophys. J. Roy. Astr. Soc. **79**, 135-152.

Crossley, D.J., 1987, The development of geophysics software for PC's: Presented at the 19th Gen. Assem., Internat. Union Geod. Geophys., Vancouver, paper SW1-2.

Ellis, R.M., Hajnal, Z. and Stephenson, R.A., 1986, PRASE 85: Crustal seismic refraction profiles in the Peace River Arch region, northwestern Alberta and northeastern British Columbia: Open file Rep. 1317, Inst. Sedimentary Petr. Geol., Geol. Surv. Can.

Fuchs, K., 1969, On the properties of deep crustal reflectors: Z. Geophys. **35**, 133-149.

Gardner, G.H.F., Gardner, L.W. and Gregory, A.R., 1974, Formation velocity and density — the diagnostic basics for stratigraphic traps: Geophysics **39**, 770-780.

Marks, L.W., 1980, Computational topics in ray seismology: Ph.D. thesis, Univ. of Alberta.

McMechan, G.A. and Mooney, W.D., 1980, Asymptotic ray theory and synthetic seismograms for laterally varying structures: Theory and application to the Imperial Valley, California: Bull. Seis. Soc. Am. **70**, 2021-2035.

Meltzer, A.S., Levander, A.R. and Mooney, W.D., 1987, Upper crustal structure, Livermore Valley and vicinity, California Coast Ranges: Bull. Seis. Soc. Am. **77**, 1655-1673.

Mereu, R.F., Wang, D., Kuhn, O., Forsyth, D.A., Green, A.G., Morel, P., Buchbinder, G.G.R., Crossley, D., Schwarz, E., duBerger, R., Brooks, C. and Clowes, R., 1986, The 1982 COCRUST seismic experiment across the Ottawa-Bonnechere graben and Grenville Front in Ontario and Quebec: Geophys. J. Roy. Astr. Soc. **84**, 491-514.

Müller, G., 1984, Efficient calculation of Gaussian-beam seismograms for two-dimensional inhomogeneous media: Geophys. J. Roy. Astr. Soc. **79**, 153-166.

Razavy, M. and Lenoach, B., 1986, Reciprocity principle and the approximate solution of the wave equation: Bull. Seis. Soc. Am. **76**, 1776-1789.

Richards, P.G., 1971, An elasticity theorem for heterogeneous media, with an example of body wave dispersion in the earth: Geophys. J. Roy. Astr. Soc. **22**, 453-472.

Sheriff, R.E. and Geldart, L.P, 1983, Exploration seismology, vol. 2: Data-processing and interpretation: Cambridge Univ. Press.

Spence, G.D., 1983, RAYAMP: An algorithm for tracing rays and calculating amplitudes in laterally varying media: program documentation, Univ. of British Columbia.

_____ , Clowes, R.M. and Ellis, R.M., 1985, Seismic structure across the active subduction zone of western Canada: J. Geophy. Res. **90**, 6754-6772.

_____ , Whittall, K.P. and Clowes, R.M., 1984, Practical synthetic seismograms for laterally varying media calculated by asymptotic ray theory: Bull. Seis. Soc. Am. **74**, 1209-1223.

Valasek, P.A., Hawman, R.B., Johnson, R.A. and Smithson, S.B., 1987, Nature of the lower crust and Moho in eastern Nevada from "wide-angle" reflection measurements: Geophys. Res. Lett. **14**, 1111-1114.

Whittall, K.P. and Clowes, R.M., 1979, A simple, efficient method for the calculation of travel times and ray paths in laterally inhomogeneous media: J. Can. Soc. Expl. Geophys. **15**, 21-29.

Young, G.B. and Braile, L.W., 1976, A computer program for the application of Zoeppritz's amplitude equations and Knott's energy equations: Bull. Seis. Soc. Am. **66**, 1881-1885.

Zelt, C.A. and Ellis, R.M., 1988, Seismic structure of the crust and upper mantle in the Peace River Arch region, Canada: J. Geophys. Res., submitted.